

# Giant disk galaxies : Where environment trumps mass in galaxy evolution

H.M. Courtois<sup>1\*</sup>, D. Zaritsky<sup>2</sup>, J.G. Sorce<sup>1</sup> and D. Pomarède<sup>3</sup>

<sup>1</sup>Université Lyon 1, CNRS/IN2P3, Institut de Physique Nucléaire, Lyon, France

<sup>2</sup>Steward Observatory, University of Arizona, Tucson, AZ, 85721, USA

<sup>3</sup>CEA/IRFU, Saclay, 91191 Gif-sur-Yvette, France

February 2015

## ABSTRACT

We identify some of the most HI massive and fastest rotating disk galaxies in the local universe with the aim of probing the processes that drive the formation of these extreme disk galaxies. By combining data from the Cosmic Flows project, which has consistently reanalyzed archival galaxy HI profiles, and  $3.6\mu\text{m}$  photometry obtained with the *Spitzer Space Telescope*, with which we can measure stellar mass, we use the baryonic Tully-Fisher (BTF) relationship to explore whether these massive galaxies are distinct. We discuss several results, but the most striking is the systematic offset of the HI-massive sample above the BTF. These galaxies have both more gas and more stars in their disks than the typical disk galaxy of similar rotational velocity. The “condensed” baryon fraction,  $f_C$ , the fraction of the baryons in a dark matter halo that settle either as cold gas or stars into the disk, is twice as high in the HI-massive sample than typical, and almost reaches the universal baryon fraction in some cases, suggesting that the most extreme of these galaxies have little in the way of a hot baryonic component or cold baryons distributed well outside the disk. In contrast, the star formation efficiency, measured as the ratio of the mass in stars to that in both stars and gas, shows no difference between the HI-massive sample and the typical disk galaxies. We conclude that the star formation efficiency is driven by an internal, self-regulating process, while  $f_C$  is affected by external factors. Neither the morphology nor the star formation rate of these galaxies is primarily determined by either their dark or stellar mass. We also found that the most massive HI detected galaxies are located preferentially in filaments. We present the first evidence of an environmental effect on galaxy evolution using a dynamical definition of a filament.

**Key words:** galaxies: evolution;

## 1 INTRODUCTION

How galaxies form and evolve remain open questions. Models reproduce global properties of galaxies well, partly by construction, but discriminative tests of plausible models are few and far between. The greatest tests of theories and models often come from considering the extremes of parameter space. For example, some of the most demanding tests on the current paradigm of structure formation come from the lowest mass galaxies, which appear to be staggeringly underabundant (the “missing satellite problem”; Moore et al. 1999; Klypin et al. 1999).

Here we focus on the opposite extreme by examining some of the most massive galaxies. Rather than considering their numbers as a population, we will examine their internal structure. While the least massive galaxies test certain aspects of the standard paradigm, namely the low mass end of the halo mass function, the nature of parent vs. satellite galaxy, and the role of reionization, giant galax-

ies help test the effects and results of a Hubble time of accretion, merging, collisions, and cannibalisms of dwarf companions (cf. Wang et al. 2011).

In a theoretical framework of structure growth whose principal characteristic is hierarchical accretion, it is natural to suspect that the environment in which a galaxy resides plays a prominent role in its evolution. However, the success of models in which observable galaxy properties (luminosity, color, morphology) are based primarily on the galaxy’s stellar or dark matter mass (see for examples the large literature on halo occupancy models, some examples include Peacock & Smith 2000; Berlind & Weinberg 2002; Conroy & Wechsler 2009) has been interpreted as supporting the view that environment plays a subdominant role in galaxy evolution (Kauffmann et al. 2003; Bundy et al. 2006).

That is not to say that environment plays no role in such models. The parent vs. satellite nature of a galaxy (cf. Berlind et al. 2005; Tinker et al. 2012) is envisioned to be key to explaining some critical observations (Peng et al. 2012; Knobel et al. 2013). However, disentangling the physics involved is complicated greatly by

\* E-mail: h.courtois@ipnl.in2p3.fr

the different degrees to which environment correlates with various galaxy properties, such as morphology and color (Blanton et al. 2003). And so, efforts to include environmental influences in models increase the complexity and complicate interpretations of the data (cf. Wechsler et al. 2006; Tinker et al. 2012; Woo et al. 2013).

Empirically, the role of environment in galaxy evolution is often explored in the densest environments (see Boselli & Gavazzi 2006, for a review), which are necessarily the most complicated. Furthermore, the principal influence of the environment may not be direct, through phenomenon such as ram pressure stripping or tidal interactions, but rather indirect through either “assembly bias” (Sheth & Tormen 2004; Gao et al. 2005; Wechsler et al. 2006), which is purely a dark matter halo phenomenon in which close halo pairs tend to have earlier formation times than otherwise similar distant pairs, and “history bias”, in which the formation age of halos *and* their subsequent star formation history varies across environments (De Lucia et al. 2012). Identifying clean tests of the influence of mass and environment on galaxy evolution is imperative.

Defying the developed expectation that mass is universally the dominant determinant of a galaxy’s appearance and that massive galaxies should not contain cold gas and not be actively star forming (cf. Dekel & Birnboim 2006; Cattaneo et al. 2006) is a class of massive, rotation dominated galaxy that includes HIZOA J0836-43, the most HI-massive galaxy known (Sc,  $M_{HI} = 7.5 \times 10^{10} M_{\odot}$ ; Haynes et al. 2011), the fastest known rotator UGC 12591 (S0/a,  $V_{max} = 506 \text{ km s}^{-1}$ ; Giovanelli et al. 1986), and a few other giant disks found in the recent 40% release of the ALFALFA survey (Haynes et al. 2011). However, these are rare galaxies. Current determinations of the local galaxy HI-mass function illustrate that statistically, HIZOA J0836-43 should not exist in the volume explored (probability of  $3 \times 10^{-8}$ ; Zwaan et al. 2005). Nevertheless, such extreme galaxies do exist, they are as massive as corresponding massive early-type galaxies at low redshift (Bernardi et al. 2011), and they provide evidence by example against the hegemony of mass in determining a galaxy’s properties.

Although such galaxies would clearly not be predicted in a model where mass alone determines a galaxy’s properties, we do not know whether more sophisticated models that are currently available successfully predict the properties of such extreme objects. Because these objects are rare, global statistical tests of the models (cf. Obreschkow et al. 2013) may not recognize the absence of such galaxies. It is therefore critical to complement large-scale comparisons, which offer the powerful advantage of statistics, with carefully crafted samples that aim to challenge the models at the margins.

These unusual galaxies must have experienced a strikingly different evolutionary history than that of massive early type galaxies, whether that means fewer or no large accretion events, a different angular momentum accretion history, and/or a distinctly different star formation history. They are likely to be the nearest analogs of the “classical” view of galaxy formation (Eggen et al. 1962), where galaxies form smoothly within an overdensity. In fact, to produce disk-dominated galaxies numerical simulations of spiral galaxies set in a cosmological context have had to select to model systems in underdense environments, a reflection on what is now understood to relate to the details of the angular momentum accretion history (cf. Governato et al. 2007; Sales et al. 2012). Therefore, the importance of environment in the genesis of these galaxies is hard-wired into detailed physics-oriented models, in opposition to what is often done in statistically-oriented theoretical treatments.

Complementing the morphological differences between early

and late type giant galaxies, there are differences in star formation histories. Late type giant galaxies presumably provide a measure of the quiescent mode of star formation and a contrast to what is likely to have occurred in early type systems. Empirically, we need to determine whether these differences are reflected in the overall star formation efficiency, which can be defined either relative to the total “condensed” baryonic content (the mass in stars and cold gas within the disk) or to the total mass. The former measures the fraction of all “condensed” baryons that formed stars, while the latter measures the fraction of the total mass converted to stars and so includes any variations in the “condensed” baryon fraction among galaxies.

At this point, we pause to consider the ill-defined, and often ill-measured, description of a galaxy’s mass. Theoretically, the preference would be to describe galaxies by their total mass, where total refers to both dark and baryonic mass, or halo mass, where halo refers to the dominant dark matter component. Even there, these are moving targets because of the definition of an outer radius, such as a virial radius. However, such definitions are completely impractical in an empirical sense because we rarely have any direct measurements of an individual galaxy’s total or halo mass. Instead, investigators either default to estimating the baryonic mass, which can be problematic in its own ways (as discussed next), or to assuming that the ranking between baryonic (or, typically, more accurately stellar) mass and halo mass is nearly 1:1 (see, for examples, halo abundance matching schemes; Berlind & Weinberg 2002). The latter approach has worked well in reproducing statistical measurements of galaxy populations from theoretical dark matter distribution models, lending support to the hypothesis that the rankings are not grossly different than 1:1. We will therefore measure baryonic masses, and presume that these are not only measurements of the baryons in these systems but also, in a ranked sense, measurements of the total mass.

The baryonic mass measurements come with their caveats as well. It is usually the case that only stellar mass, through luminosity and colors, is estimated and corrections for baryons in other phases are either ignored or treated in the mean. We will describe a somewhat more accurate process in which we use IR magnitudes that have been carefully calibrated to stellar masses and complement those with measurements of the gaseous baryons based on HI observations. This approach still ignores baryons in hot phases and there is a well-known baryon shortfall (Bregman 2007), so these masses are still not the full picture. However, to be specific, we will measure the stellar plus gaseous masses, and use these liberally as a proxy for the total galaxy mass. This assumption is broadly valid, not worse than a factor of two in total mass, as evidenced by the scatter about an apparently constant baryon fraction resulting from studies of the baryonic Tully-Fisher relation (Zaritsky et al. 2014b) for galaxies spanning many decades in baryon mass.

The Cosmic Flows project, which is consistently remeasuring all available HI line widths, provides a uniform, unprecedented dataset from which to draw these massive rotating and HI-massive galaxies. In combination with the infrared imaging provided by the *Spitzer Space Telescope* and the calibrated conversion between 3.6 photometry and stellar mass (Eskew et al. 2012), we are now in a position to compare gaseous, stellar, and total masses for these rare rotationally supported giant galaxies. In §2 we present the data and present our two subsamples of extreme galaxies in §3. In §4 we examine the properties of these galaxies relative to the baryonic Tully-Fisher relation and draw inferences regarding the “condensed” baryon fractions and star formation efficiencies. We sum-

marize our conclusions in §5. Where needed, we adopt  $H_0 = 70 \text{ km s}^{-1} \text{ Mpc}^{-1}$ .

## 2 THE DATA

### 2.1 The Cosmic Flows Program

Since 2009, the Cosmic Flows project (CF) has gathered all the digital HI spectra available from public archives of the largest radio-telescopes worldwide and measured them in a consistent way. Two sub-projects of CF, at Green Bank in the USA and at Parkes in Australia (Courtois et al. 2011), complete the archives for targets without previous observations adequate for the Tully-Fisher method of distance measurements (Tully & Fisher 1977). The latest update of this catalog is published in Courtois & Tully (2015).

The main goal of CF is to map the all-sky peculiar velocity field locally and to uncover, at high spatial resolution, the underlying dark matter distribution. In that cause, they have measured tens of thousands of galaxy line widths with a new method described by Courtois et al. (2009) and Courtois et al. (2011). Briefly, for each galaxy, they evaluate the line width parameter  $W_{m50}$ , which measures the HI profile width at 50% of the mean flux within the velocity range encompassing 90% of the total HI flux. That quantity is transformed into the more physically motivated parameter  $W_{mx}$ , which is the same width corrected for the slight relativistic broadening and for broadening due to finite spectral resolution, corrected for inclination and so is effectively twice the maximum rotation velocity. Technical details of this process are provided by Courtois et al. (2009) and Courtois et al. (2011), and reviewed in Tully & Courtois (2012).

The result is a catalog of HI measurements of unprecedented size (14221 galaxies) and consistency. They use the ratio of the signal level at 50% of the mean flux to the noise measured beyond the frequency extremities of the signal to parametrize the line width uncertainty. Only profiles with uncertainty estimates smaller than or equal to  $20 \text{ km s}^{-1}$  are retained (more than 75% of the 14221 galaxies, exactly 10733 galaxies satisfy this criteria) after a supplementary visual inspection. This catalog is available for public use at the Extragalactic Distance Database (EDD) website<sup>1</sup> where several other parameters, such as the integrated HI line fluxes for those lines with a flux calibration error better than about 10 to 15% and the average heliocentric velocities, are also available and described (Tully et al. 2009). In addition to this “all-digital” catalog, we also use the “pre-digital” catalog of measurements at 20% of the HI line peaks. The relation

$$V_{m50}(\text{all} - \text{digital}) = (1.015 \times W_{20}(\text{pre} - \text{digital}) - 11.25) \quad (1)$$

connects the two catalogs (Courtois et al. 2009). In total, we have 16,124 galaxies with coherent HI measurements and 12,189 with sufficiently good quality for distance measurements.

### 2.2 The Infrared Data

We use  $3.6\mu\text{m}$  magnitudes measured from data obtained using the *Spitzer Space Telescope* (Werner et al. 2004) and the IRAC camera (Fazio et al. 2004), from a number of different observing programs (such as, Dale et al. 2009; Sheth et al. 2010; Sorce et al. 2012). For Tully-Fisher studies, within the CF sample, there are 6,007 galaxies with sufficiently good HI linewidth measurements,  $\sigma_{W_{m50}} < 20$

$\text{km s}^{-1}$  and inclinations greater than  $45^\circ$ . Among these, 2,493 have been observed with *Spitzer*. We adopt total magnitudes measured either using the Archangel pipeline (Schombert 2007) or the S<sup>4</sup>G pipeline (Muñoz-Mateos & et al. 2015). Distances, needed to calculate absolute magnitudes, are presumed from the Hubble flow using  $H_0 = 70 \text{ km s}^{-1} \text{ Mpc}^{-1}$  and the recessional velocities from the HI catalog.

We use the  $3.6\mu\text{m}$  photometry because there now exist simple, and robust, conversions to stellar mass (Eskew et al. 2012; Meidt et al. 2014) that have been vetted with comparisons to SDSS SED-derived stellar masses (Cybulski et al. 2014). Eskew et al. (2012) give the conversion between stellar mass and infrared flux as  $M_* = 10^{5.97} F_{3.6} (\frac{D}{0.05})^2$ , where  $D$  is the distance to the galaxy in Mpc,  $F_{3.6}$  is the flux in Jy, and  $M_*$  is expressed in solar masses. A slightly more precise estimate can be obtained by including the  $4.5\mu\text{m}$  flux, but both Eskew et al. (2012) and Querejeta & et al. (2015) find only a weak dependence between  $M_*$  and infrared color. The largest uncertainty in the derived stellar mass remains the overall normalization due to uncertainties in the adoption of a specific stellar initial mass function (the Eskew et al. (2012) calculation adopts a Salpeter IMF).

## 3 GIANT DISK GALAXIES

To define our galaxy subsamples, we search both for those galaxies with the largest HI masses and for those with the largest rotational velocities. Due to our use of the HI database, we may miss gas-poor versions of the latter, although such galaxies are likely to be early type and therefore not the pristine test cases we are searching for. Because of broad correlation between gas mass and total mass, these samples have some objects in common.

### 3.1 The most HI massive galaxies

We compute HI masses ( $M_{\text{HI}}$ ) from the publicly available integral fluxes and average heliocentric velocities (Courtois et al. 2009) using

$$M_{\text{HI}} = 2.36 \times 10^5 D^2 \text{FI} \quad (2)$$

where  $D$  is the distance in Mpc and  $\text{FI}$  is the integrated flux in the HI line in  $\text{Jy km s}^{-1}$ .

The distribution in  $\log M_{\text{HI}}$  for the 10733 galaxies for which we can calculate the necessary quantities covers the range of 5.53 to 10.72, with a median of 9.62, corresponding to a range of  $3.4 \times 10^5$  to  $5.2 \times 10^{10} M_\odot$ . PGC8681/UGC01752 is the most HI massive (Figure 1) galaxy in the full sample, but it is not in our subsample because we lack *Spitzer* photometry for it. PGC17625, with only a slightly lower HI mass ( $4.5 \times 10^{10} M_\odot$ ), tops our list. In Figure 2 we show the distribution of  $M_{\text{HI}}$  for the 100 most HI massive galaxies that also have existing *Spitzer* photometry. Choosing the top 100, which was set only because it is a simple round number, corresponds roughly to selecting the top 5% of the available sample. One galaxy (PGC90167) was removed from our subsample because even though it was observed with *Spitzer*, the S<sup>4</sup>G survey (Sheth et al. 2010; Muñoz-Mateos & et al. 2015) was unable to provide a reliable magnitude measurement.

We distinguish this sample from an HI rich sample, where in that case one would presumably select on either the ratio of gas to stellar mass,  $M_{\text{HI}}/M_*$ , or to dark matter mass,  $M_{\text{HI}}/M_{\text{DM}}$ . Although

<sup>1</sup> <http://edd.ifa.hawaii.edu>; catalog “All Digital HI”

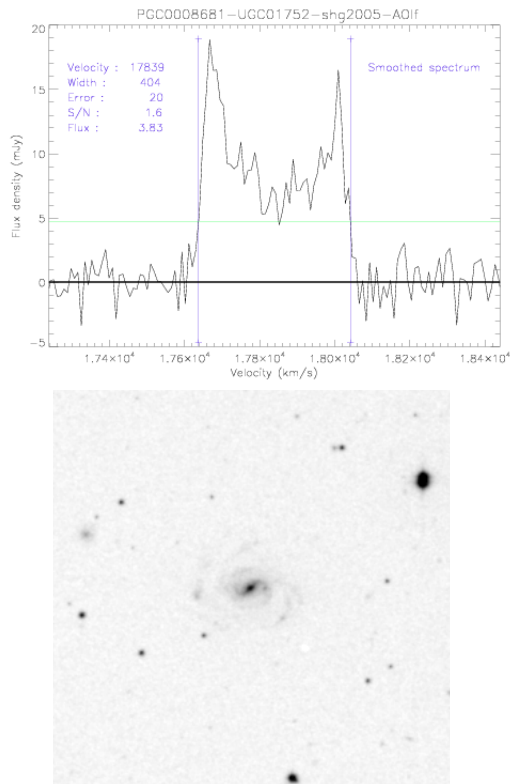


**Figure 1.** HI profile of PGC0008681 as observed at Arecibo, and B band image from DSS2 survey at the size of Arecibo beam (3 arcmin). This is the largest HI mass galaxy recorded in the full available sample, but is not in our subsample due to lack of *Spitzer* photometry.

such a sample is also of interest, that selection depends on the modeling of  $M_*$  or  $M_{DM}$  and therefore complicates any interpretation.

### 3.2 The fastest rotators

Our rotational velocities come from the  $W_{mx}$  parameter:

$$v_{rot} = \frac{W_{mx}/2}{\sin(i)} \quad (3)$$

where  $v_{rot}$  is the galaxy rotational velocity and  $i$  the inclination to the line of sight.

Among the full sample of galaxies (not yet implementing the *Spitzer* imaging requirement), the rotational velocities range from 11 to 514 km s<sup>-1</sup> for PGC71392/UGC12591 (see Figure 3) with a median of 145 km s<sup>-1</sup>. Again the top ranked galaxy is not in our final sample due to the lack of infrared photometry, and so the top ranked galaxy in our sample is PGC17625 with a rotation velocity of 450 km s<sup>-1</sup>. The distribution of rotational velocities of our sample is also illustrated in Figure 2.

## 4 DISCUSSION

### 4.1 The baryonic Tully-Fisher relationship

Because in any sample there will always be some galaxies with the largest HI masses or rotation velocities, we require a fiducial against which to compare these galaxies to the average galaxies.

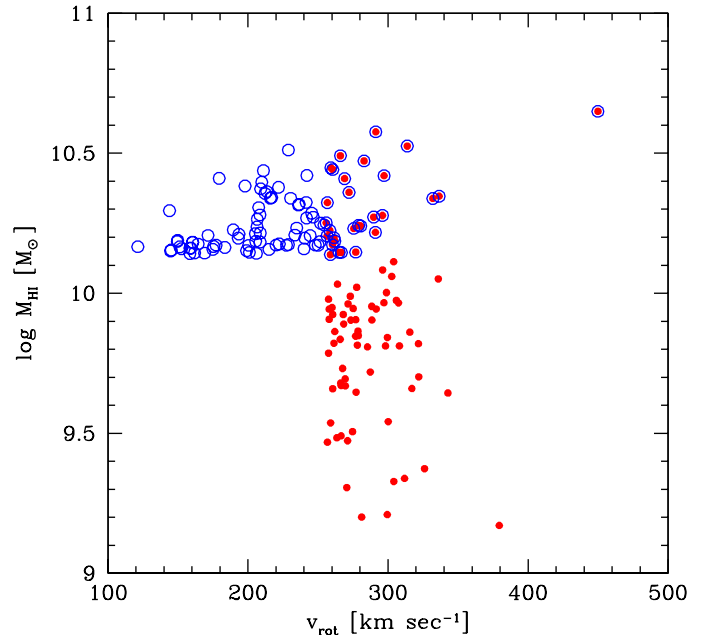


**Figure 2.** Distribution of galaxies in our subsamples selected by rotational velocity and HI mass. We highlight the HI mass selected sample using open blue circles and the rotational velocity selected sample using filled red circles. We will continue this color scheme throughout the paper to differentiate the samples. There are 26 galaxies in common between the two samples.

Are they simply scaled up versions of lesser galaxies or are they otherwise distinct?

This class of question can be addressed using galaxy scaling relations. For rotationally supported galaxies the most commonly used such relation is that identified by Tully & Fisher (1977), which relates rotational velocity to optical luminosity. One can then use such a relation to ask such questions as whether these galaxies have unusual luminosities for their rotational velocities.

Since the original work, this scaling relation has been extended in one key way that has been shown to be particularly necessary for lower mass galaxies, namely the substitution of the baryonic mass in place of the luminosity (Freeman 1999; Walker 1999; McGaugh et al. 2000; Verheijen 2001; Geha et al. 2006). For our purposes, we will use the baryonic Tully-Fisher (BTF) measured for S<sup>4</sup>G galaxies (Zaritsky et al. 2014b) as our fiducial because the data used to establish that relation are most comparable to the data presented here.

To implement the BTF we require measurements of the stellar and gaseous masses. We described in §2.2 how we obtain  $M_*$ .

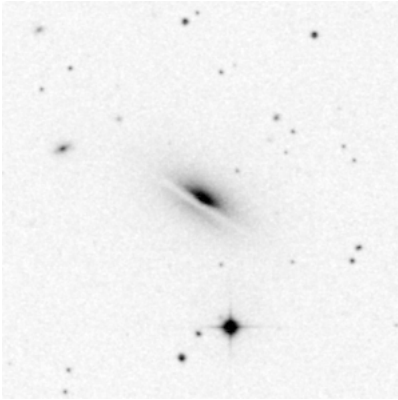
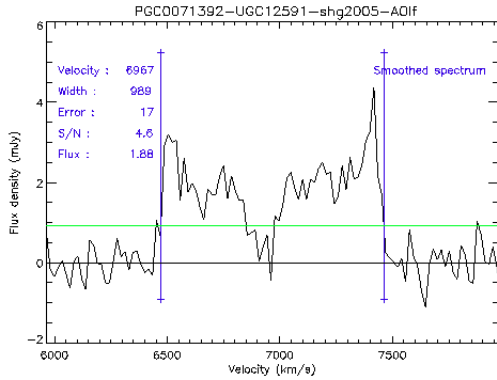


**Figure 3.** HI profile of PGC0071392 as observed at Arecibo, and B band image from DSS2 at the size of Arecibo beam (3 arcmin). This is the largest rotational velocity recorded in the full available sample, but is not in our subsample due to lack of *Spitzer* photometry.

Obtaining a measurement of the gaseous mass,  $M_{\text{GAS}}$ , involves correcting the HI mass for the missing He, other “metals”, and molecular gas. This is done here as described by Zaritsky et al. (2014b) to enable a direct comparison to their results. The baryonic mass is then simply  $M_* + M_{\text{GAS}}$ . As noted by those authors, this quantity is more accurately referred to as the “condensed” baryonic mass because it only represents the baryons that have settled into the disk of the galaxy and is missing the possibly substantial baryonic components in the halos of these galaxies.

In Figure 4 we present our first comparison of the properties of the giant galaxies to the more general population. As shown, both the fastest rotators and most HI massive galaxies lie generally on the BTF relation, although some differences exist. First, although slightly difficult to notice from this Figure but easier to spot in Figure 5 where we plot the residuals from the mean BTF ( $\Delta\text{TF}_{\text{Baryons}}$ ), the fastest rotators fall somewhat below the mean trend as depicted by the red line in Figure 4. Second, and much clearer, the HI-massive sample lies systematically above the line. The one striking outlier, PGC90167, has a T-Type = -2. Because it is such an early-type galaxy, its dynamical support is probably not dominated by rotational support and therefore the galaxy should not be expected to satisfy the BTF (it has a low  $v_{\text{rot}}$  of 45 km s<sup>-1</sup>). We remove this one galaxy from further consideration, leaving both the fast rotator and HI-massive samples with 99 galaxies, and proceed to discuss

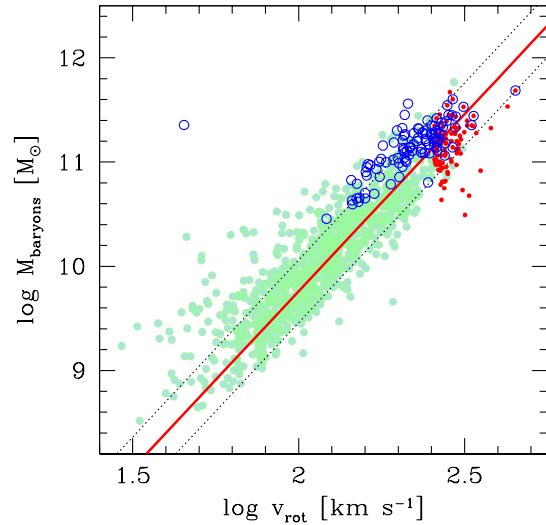


**Figure 4.** Baryonic Tully Fisher. Comparison of the BTF for the S<sup>4</sup>G sample and our subsamples of extreme disks. The red filled circles represent the fast rotators, while the blue open circles represent the HI-massive galaxies. The red solid line is described in detail by Zaritsky et al. (2014b) but in brief represents a model where a fixed fraction ( $\sim 0.4$ ) of the baryons in a halo of circular velocity of  $v_{\text{rot}}$ , which has the cosmological baryon fraction, are settled in the disk. As shown by those authors, this simple model is consistent with the empirical best fit line. The dotted lines represent factors of two change in that fixed fraction.

the two subsamples and their location relative to the mean BTF relation.

There are a variety of potential explanations for why the fast rotators fall below the mean BTF:

First, this result could be a manifestation of a Malmquist-like bias. Because we select this subsample using  $v_{\text{rot}}$ , errors that artificially inflate  $v_{\text{rot}}$  will preferentially contaminate our sample with galaxies that appear to be “baryon poor” for their rotation velocity. The mean of the distribution (Figure 5) is displaced by  $\sim 0.15$  dex, suggesting that we would need to have a similar magnitude error in  $v_{\text{rot}}$  for this to be a plausible explanation. That level of error translates to an error of  $\sim 40\%$  or over 100 km s<sup>-1</sup> for  $v_{\text{rot}} = 300$  km s<sup>-1</sup>. Given our demands on precisely determined HI widths and high inclinations, this level of error seems unlikely.

Second, inclination errors, in the form of an underestimation of the true inclination, could lead us to preferentially place objects to the right of the mean BTF. We test for this effect by searching for a correlation between inclination and  $\Delta\text{TF}_{\text{Baryons}}$ . There is only a very weak positive correlation (positive is in the necessary sense) that is entirely consistent with arising at random (can be rejected as arising randomly with only 37% confidence). We conclude there

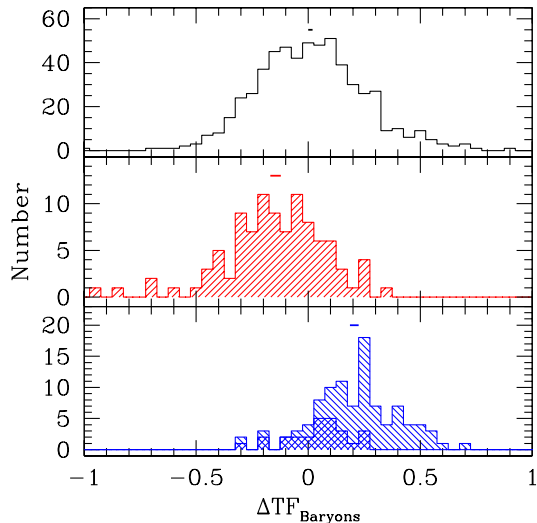


**Figure 5.** Deviations from the mean BTFR relation,  $\Delta TF_{\text{Baryons}}$ , for the BTFR shown in Figure 4, for galaxies with  $v_{\text{rot}} > 2$ . Upper panel shows the residual distribution for the S<sup>4</sup>G sample from Zaritsky et al. (2014b), middle panel for our subsample of fast rotators, and lower panel for our subsample of HI-massive galaxies. Also shown in the lower panel, with the opposite hashing is the subpopulation of HI-massive galaxies that are also in the fast-rotator sample. The small horizontal bars placed above each histogram represent the mean of each distribution and the length represents the standard deviation of that mean.

is no evidence that inclination is systematically affecting the BTFR residuals of the high  $v_{\text{rot}}$  galaxies.

Third, at these high  $v_{\text{rot}}$  values we may have a larger fraction of galaxies for which pressure supported components play a larger dynamical role. Noordermeer & Verheijen (2007), when examining the high mass end of the Tully-Fisher (TF) relation, found that a number of their galaxies were S0/Sa types (as well as finding a similar displacement of these massive galaxies below the general TF). When dealing with such galaxies a number of investigators (Burstein et al. 1997; Weiner et al. 2006; Kassin et al. 2007; Zaritsky et al. 2008) have suggested combining the use of  $v_{\text{rot}}$  and velocity dispersion,  $\sigma$ , into a single kinematic term that measures the full dynamical support. While this may be appropriate when observing stellar components, it is not for gaseous measurements (there is negligible pressure support of the gas component and, even if there were, such a correction would move these galaxies even further to the right in the Figure). If one does attribute the dip below the BTFR for this subsample to the prevalence of early-type galaxies at these rotation velocities, the cause of the dip would have to be a general failure of (or departure from) the linear BTFR, rather than from the omission of  $\sigma$  in the evaluation of the dynamical support.

Fourth, the intrinsic BTFR may deviate from a straight line. Numerical

simulations (Aumer & White 2013) also find that the most massive galaxies tail off below the BTFR (Zaritsky et al. 2014b) and so this phenomenon may be a natural result, for which an intuitive explanation might provide significant insight to the nature of galaxy formation. As a potentially interesting aside, massive early type galaxies also appear to fall below their analogous scaling relation, the Fundamental Plane (Bernardi et al. 2011). As for the early types, for which curvature in the scaling relation is established (Zaritsky et al. 2006; Bernardi et al. 2011), a unified scaling relation (Zaritsky et al. 2008; Zaritsky 2012) would imply the same phenomenon for late types.

Finally, the position of these galaxies may indicate that the stellar mass has been underestimated in these systems relative to that of the lower  $v_{\text{rot}}$  systems. This error could arise because the stellar initial mass function (IMF) is more bottom heavy in the faster rotators. Although this hypothesis may seem farfetched, there is empirical evidence for this type of behavior among early type galaxies (van Dokkum & Conroy 2010; Cappellari et al. 2012), where the IMF becomes progressively more bottom heavy as one considers galaxies with larger velocity dispersions. Evidence for IMF variations even extends to Local Group clusters (Zaritsky et al. 2012, 2014a), and so the possibility that such variations exist among disk galaxies as well should not be quickly dismissed.

As already mentioned, the more striking departure from the BTFR is seen for the HI-massive subsample. Here the departure, shown clearly in Figures 4 and 5, can be interpreted to mean that these galaxies have a larger fraction of their cosmologically apportionment of baryons within their disks, as stars or gas, than the typical disk galaxy. As with the fast rotator sample, there are a set of potential systematic errors that could also produce this result:

First, one might wonder whether this could be the result of a Malmquist-like bias. We select systems with large HI masses, and therefore errors in the measured HI mass could both help populate the sample and make it appear as if these galaxies are HI rich for their rotation velocity. However, these galaxies also have larger stellar masses than typical, as shown in Figure 6 where we compare to a stellar mass only version of the BTFR (renormalized to produce a mean departure of zero for galaxies with  $\log v_{\text{rot}} > 2$  in S<sup>4</sup>G). Because the stellar masses, and this stellar version of the BTFR, are entirely independent of  $M_{\text{HI}}$ , we conclude that the departure of these galaxies from the BTFR is not a result of errors in the HI measurements themselves.

Second, errors in the adopted distance would affect both the gaseous and stellar masses because distance plays a role in converting between observables and masses. The mean shift between either the gaseous or stellar masses and the fiducial of the S<sup>4</sup>G sample is  $\sim 0.22$  dex (see Figures 5 and 6). Because both mass estimates are proportional to  $D^2$ , this offset corresponds to a systematic offset of 0.11 dex in  $D$  or alternatively a 30% error. We know such an error cannot arise from  $H_0$  given the current degree of uncertainty in the Hubble parameter (Freedman & Madore 2010). Peculiar motions could be as large as several thousand  $\text{km s}^{-1}$  in the richest galaxy clusters, but are typically a few hundred  $\text{km s}^{-1}$  (Peebles 1976; Kaiser 1987), particularly in the low density environments that these galaxies reside in. One might dismiss peculiar motions on the basis that these should result in increased scatter rather than an offset, but recall that we select the most HI massive galaxies, and therefore are predisposed toward galaxies with overestimated distances. However, even with peculiar motions that are as large as 500  $\text{km s}^{-1}$ , the induced error is  $< 30\%$  in 97 out of the 99 galaxies in the HI-massive sample. We conclude that distance errors are not

responsible for the systematic offset of HI massive galaxies from the BTF.

Third, inclination errors will affect  $v_{rot}$ . However, unlike in the previous discussion, inclination does not play a role in the selection of these galaxies (other than the requirement that they be inclined by more  $45^\circ$ ). As before, we test for the influence of inclination by searching for a correlation between measured inclination and the offset from the BTF. Again we find no significant correlation (the probability of the observed correlation arising at random is 18%). We conclude that inclination errors are not driving the BTF residuals.

Finally, the adopted relation between  $v_{rot}$  and halo mass may be incorrect. We have taken a mean trend from Bullock et al. (2001), normalized using the Milky Way (see Zaritsky et al. 2014b), but different types of galaxies will have different degrees of adiabatic contraction, and therefore different relations between the inner rotation curve,  $v_{rot}$ , and the characteristic halo circular velocity,  $v_c$ . A factor of two overestimation in the fraction of baryons within the halo that have settled into a disk,  $f_c$ , would arise if we had underestimated the halo mass of galaxies in our subsample by a factor of two, or alternatively underestimated  $v_c$  by  $\sqrt{2}$ . Because it is difficult to imagine a scenario by which  $v_{rot}$  is smaller than that due to the dark matter, we would posit that the problem, if it exists at all, is that the  $v_c$  of the typical galaxies are overestimated by a factor of  $\sqrt{2}$ . For a typical galaxy in our sample with  $v_{rot} \sim 180 \text{ km s}^{-1}$ , the necessary error would require the halo to have  $v_{rot} \sim 127$ . Such a steep drop between  $v_{rot}$  and  $v_c$  is not found in dynamical analyses (Zaritsky & White 1994) or gravitational lensing (Fischer et al. 2000). While the conversion between  $v_{rot}$  and  $v_c$  has its associated systematic uncertainties, we conclude that it is unlikely to globally cause a factor of two increase in the apparent  $f_c$  of the HI massive galaxy sample.

In the upper panel of Figure 7, we calculate how the BTF offset translates into differences in the level of baryon “condensation” in galaxies (see Zaritsky et al. 2014b, for the original discussion of this term and the calculation relative to the BTF) as a function of  $v_{rot}$ . In other words, the Figure shows the fraction of baryons — stars and gas — apportioned to a given halo at the level of the universal baryon fraction that settle into the disks of these galaxies. In the lower panel of the same Figure, we plot the star formation efficiency, or alternatively the fraction of the “condensed” mass that is turned into stars,  $f_* \equiv M_*/(M_* + M_{GAS})$ .

The HI massive galaxies are clearly distinct from the typical disk galaxy in that the fraction of condensed baryons, which in some cases reaches nearly 100% of the cosmological baryon fraction (meaning that all of the baryons expected in a halo of the given mass are in gas and stars within the disks), is significantly larger over nearly the full range of  $v_{rot}$ . We speculate that the reason that the difference becomes less striking at higher  $v_{rot}$  is that the HI mass limit on which we select these galaxies is approaching the typical HI mass for these more massive galaxies.

In contrast, the star formation efficiency is remarkably similar for the HI massive galaxies and typical  $S^4G$  galaxies, even as that efficiency appears to depend on  $v_{rot}$ . The rise in  $f_*$  is interesting but difficult to interpret because it probably also reflects a change in the morphological mix of galaxies. It is nevertheless, particularly interesting that among the HI massive galaxies, the efficiency follows that of the  $S^4G$  galaxies despite variations of a factor of two in  $f_c$ . This result suggests that star formation is strongly governed by the available gas mass and internal regulation, a result that is at least broadly reminiscent of results obtained in detailed studies of

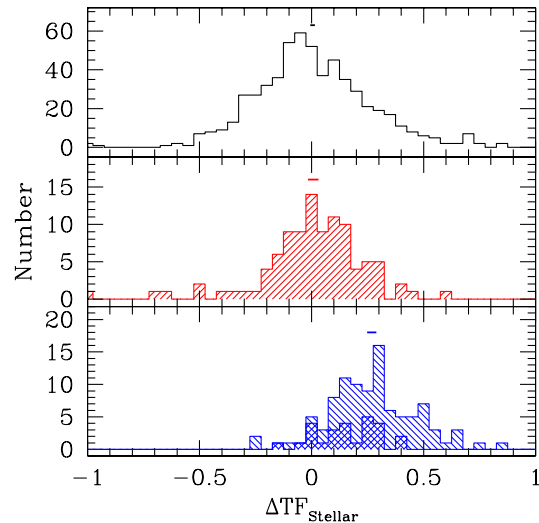


**Figure 6.** Deviations from the stellar mass Tully-Fisher relation,  $\Delta TF_{Stellar}$ , where the stellar TF is in effect the classic TF because the stellar masses are recovered directly from the luminosities. Panels and lines indicating means of the distribution are as in Figure 5. The deviation of the HI selected galaxies is as strong as in Figure 5 even though these residuals are independent of HI mass.

star formation rates in galaxies (Kennicutt & Evans 2012), rather than external factors.

## 4.2 Environment

Given our general understanding that massive galaxies tend to be early types, the physically interesting question is why the massive galaxies we have selected are such strong examples of late type galaxies. If the two primary drivers of galaxy evolutionary differences among galaxies are mass and environment, and if mass is not the cause of the differences seen here, then environment has somehow played a dominant role for these galaxies. Confirming this conclusion is, however, difficult. By the nature of the selection of the sample (isolated so that the HI beam is clean and the result is a well-defined double horned profile), we have already selected against galaxies in dense environments. Upon examination, we confirm that none of these galaxies is in a highly overdense environment, such as an Abell cluster. Looking a bit further, we searched for differences in the environments of these galaxies relative to galaxies in the 2MASS redshift catalog (2MRS) (Huchra et al. 2012) by comparing the correlation function of our galaxies to that of similar galaxies in the redshift catalog. We found no convincing evidence of a difference.

We face two difficulties in exploring the role of environment further. First, environment means many different things. The local

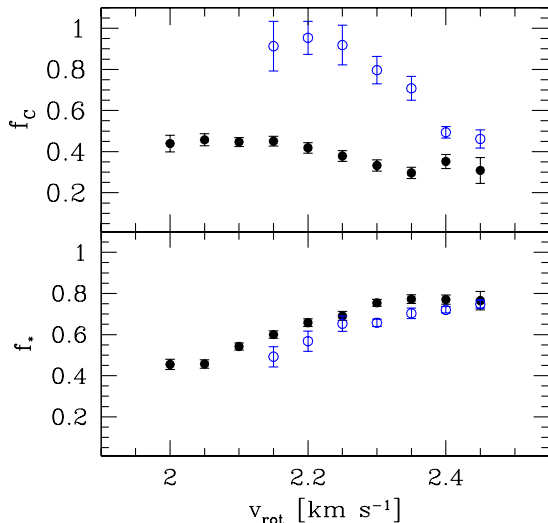


**Figure 7.** The condensed baryon fraction,  $f_c$ , which is defined as the fraction of all the cosmologically expected baryons in a halo that are present in the disk as either cold gas or stars, as a function of  $v_{rot}$  (upper panel) and the star formation efficiency,  $f_*$ , which is defined as the fraction of condensed baryons that are in stars ( $M_*/(M_* + M_{GAS})$ ). In this figure blue open circles represent the HI selected sample and black filled circles represent the S<sup>4</sup>G sample. Points only plotted if bin has at least 3 galaxies in it. Error bars represent error in the mean.

environment, whether a galaxy is a parent or satellite, appears to play an important role in the observable characteristics of galaxies (Berlind et al. 2005; Tinker et al. 2012). On the other hand, the large scale (several Mpc) environment also appears to play a role (Gómez et al. 2003). Therefore, any one measure of environment will be a far from perfect diagnostic of the role of environment in evolution. Second, galaxies, particularly most massive galaxies, have inhabited many different environments over their lifetime. The environment we measure today, especially for those in denser than average environments, is not a complete measure of the environmental history of a galaxy (De Lucia et al. 2012). Both of these issues suggest that standard analyses may at best yield only subtle differences, even if environment does play a role in a galaxy’s evolution.

To pursue this topic further, we explore a novel characterization of environment using the local shear field, as used for the Laniakea discovery (Tully et al. 2014). A Wiener Filter reconstruction applied to the Cosmicflows-2 database (Tully et al. 2013) recovers the underlying 3D velocity field with an effective resolution of a few Megaparsecs (Courtois et al. 2012). By taking spatial derivatives of the velocity field, we compute the dimensionless shear tensor. The tensor’s eigenvalues ( $\lambda_1, \lambda_2, \lambda_3$ ) describe the strength (relative to the Hubble expansion) of compression (positive values) or

expansion (negative values) along the eigenvectors of the shear:  $\hat{e}_1$ ,  $\hat{e}_2$ , and  $\hat{e}_3$ . At each position in space, we calculate the three eigenvalues of the velocity shear tensor. By ordering these eigenvalues from most positive to most negative, we set thresholds that capture four possibilities. Flows can be inward on all three axes, the condition of a cluster, inward on two axes and outward on the third, the condition of a filament, inward on one axis and outward on two, hence a sheet, or outward on all three axes, hence a void. We define boundaries around contiguous regions with the same shear properties and the contours outline the cosmic web as reconstructed by the V-web algorithm (Hoffman et al. 2012). The statistical uncertainty of the shear eigenvectors and eigenvalues are controlled by means of an ensemble of constrained realizations. The spatial cosmography and reconstructed velocity field of the giant galaxies’ environment is shown in Figure 8.

We compute the number of galaxies in cells that are classified as knots, filaments, sheets, or nothing (voids or no signal) for two redshift catalogs V8K (Courtois et al. 2013) (the most complete redshift catalog within 8,000 km/s) and 2MRS (Huchra et al. 2012). Some of the studied volume is without signal (for example the zone of avoidance). It is classified as a void in the V-web, but we do not have galaxies there. By confining the analysis to within 8000 km/s, our samples of HI massive and fast rotators now contain 18 and 17 galaxies, respectively, see Tables 2, 3 and 4. As seen in Table 1, our HI giant galaxies live preferentially in filaments: 10 out of 18 (56%) while only 21% of all galaxies within the same volume located today in a filament. Filaments represent 10% of the volume, contain 21% of all galaxies, and 56% of the giants. Adopting a binomial distribution with the probability of a “true” output (filament) defined to be 0.21, we find that the probability of having 10 or more “true” outcomes is 0.00025. so the signal is significant at greater than  $3\sigma$  confidence. In contrast, although our fast rotators also show a hint of a preference for filaments, there the result is only statistically significant at  $\sim 1\sigma$  confidence.

## 5 CONCLUSIONS

We investigated the properties of galaxies that potentially challenge the current paradigm of galaxy evolution. Albeit rare, these massive disk galaxies run counter to the idea that mass alone determines a galaxy’s star formation rate or its morphology. Of course there are other previously known reasons to disfavor such an extreme view, but well-specified, carefully defined samples have the potential to highlight these discrepancies. We selected the 100 most HI massive galaxies and the 100 most rapidly rotating disk galaxies from HI catalogs available for public use at the Extragalactic Distance Database that contains thousands of coherently measured HI profiles.

To compare with the overall disk population, we use the baryonic Tully-Fisher (BTF) relation as a benchmark. That relation holds broadly because a nearly constant fraction of the available baryons in each galaxy’s halo settle into the disk (Zaritsky et al. 2014b). The classic Tully-Fisher (TF) relation then holds because for most galaxies a fixed fraction of those settled, or “condensed”, baryons turn into stars. Deviations from the BTF therefore indicate a variation in the fraction of condensed baryons,  $f_c$ , which could signal interesting evolutionary deviations from the typical galaxy. Deviations from the TF relation could similarly signal deviations  $f_c$ , or they could signal deviations in the star formation efficiency.

Using the HI data in combination with available  $3.6\mu\text{m}$  photometry from *Spitzer* observations, we place our two samples on



**Table 1.** Environmental study using the Cosmic-V-web computed within a sphere of 8,000 km/s radius. Number and percentage (respectively) of galaxies located in structures dynamically classified as knots, filaments, sheets and voids. The most massive HI galaxies are preferentially located in filaments, with a frequency that is a factor of two larger than a random galaxy.

Objects	in knots	in filaments	in sheets	in void cells
HI massive	0 (0%)	10 (56%)	4 (22%)	4 (22%)
Fast rotators	1 (6%)	5 (29%)	8 (47%)	3 (18%)
2MRS galaxies	586 (2%)	8065 (21%)	18236 (47%)	11483 (30%)
V8k galaxies	500 (2%)	6408 (21%)	14468 (47%)	9324 (30%)
Vweb cells	2459 (0.2%)	112639 (10%)	451487 (42%)	518007 (48%)

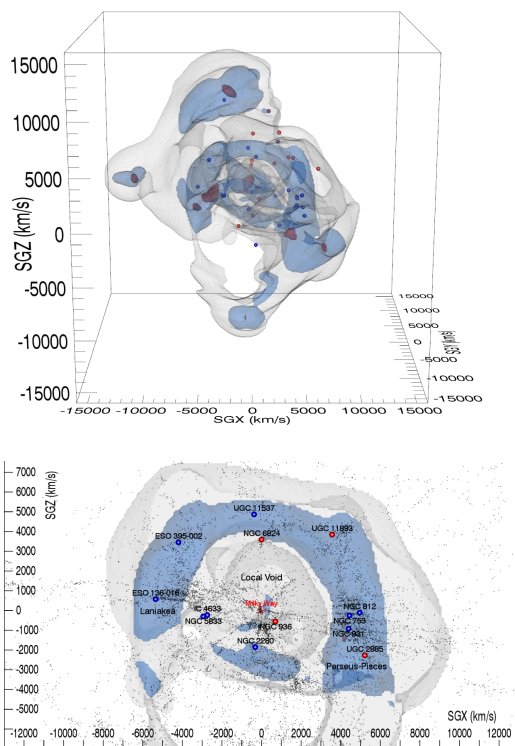


**Figure 8.** The environment is studied using the Velocity-Cosmic-Web (V-web). Regions gravitationally collapsing along one direction are sheets, along two orthogonal directions are filaments, along three orthogonal directions are knots. Regions expanding in three directions are voids. Contours in grey, blue and red are showing regions classified respectively as sheets, filaments and knots. The top panel shows a 3D view. The bottom panel is a closer view of a slice of 1000 km/s width on Supergalactic Y axis. The galaxies in 2MASS redshift catalog (2MRS) are plotted with black dots. The cosmography is given with Laniakea on the left and Perseus-Pisces supercluster on the right. The most massive HI galaxies (blue spheres) are located preferentially in filaments with a  $\sim 100\%$  higher probability than random galaxies in two different redshift catalogs, V8K or 2MRS. For the fast rotators (red spheres) we cannot confidently identify a preferred environment.

the BTF. We find both samples deviate systematically from the existing BTF. The rapid rotators tend to lie below the BTF. We discuss a number of possible reasons for this deviation, including a suggestion that the scaling relation is not linear at the massive end. Such behavior is also seen in massive early-type galaxies (Bernardi et al. 2011). The systematic deviation might also hint at bottom heavy IMFs in more massive galaxies, again as seen in massive early type galaxies (van Dokkum & Conroy 2010; Cappellari et al. 2012).

The HI massive galaxies lie systematically above the BTF. If these deviations are interpreted as variations in  $f_c$ , then we conclude that there are galaxies in which  $f_c$  approaches 1, or in other words the entire allotment of baryons for that halo have found their way to the disk. In spite of this, or whatever other process may be driving the deviation from the BTF, the star formation efficiency, when quantified as the fraction of disk baryons that are in stars, is the same in these systems as in more typical galaxies. We conclude that the star formation efficiency is driven by internal self-regulation, while  $f_c$  can be altered by external factors.

Although mass is clearly not the driver of the morphological or star formation history differences that exist between these galaxies and other similarly massive galaxies, we have not identified the driver. Our galaxies avoid the densest environments, but so do other galaxies that are not similarly extreme. When looking in detail for environmental differences, we found that the most massive HI detected galaxies are located preferentially in filaments. We present the first evidence of an environmental effect on galaxy evolution using a dynamical definition of a filament.

## 6 ACKNOWLEDGMENTS

This research has made use of the NASA/IPAC Extragalactic Database (NED) which is operated by the Jet Propulsion Laboratory, California Institute of Technology, under contract with the National Aeronautics and Space Administration. We acknowledge the usage of the HyperLeda database (<http://leda.univ-lyon1.fr>). HC and JS acknowledge support from the Lyon Institute of Origins under grant ANR-10-LABX-66 and from CNRS under PICS-06233. DZ acknowledges support from a NASA ADAP award (NNX12AE27G) and an NSF AAG grant (AST-1311326). We thank Yehuda Hoffman from the Hebrew University in Jerusalem for providing a Cosmic-V-web computation of the cosmicflows-2 database.

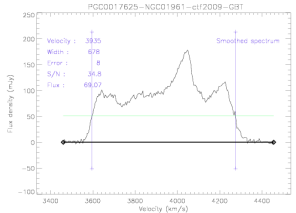
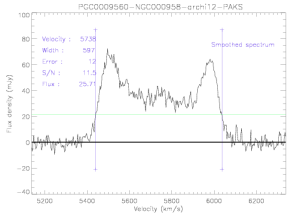
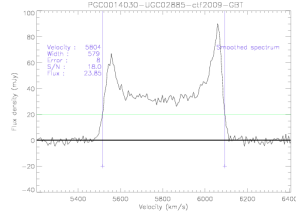
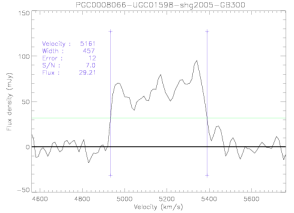
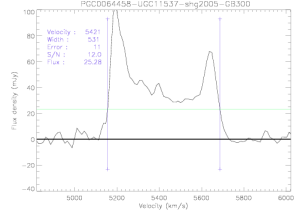
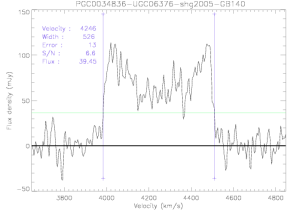
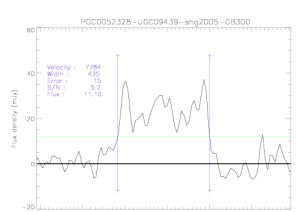
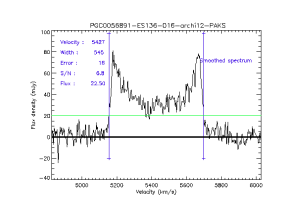
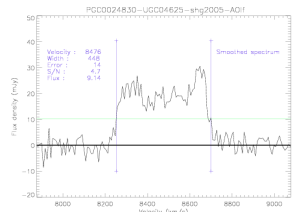
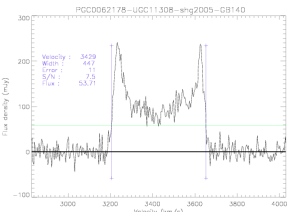
**Table 2.** The 20 largest HI-mass galaxies

PGC	Name	J2000 coordinates	$V_{\text{hel}}$ $\text{km s}^{-1}$	$W_{\text{mx}}$ $\text{km s}^{-1}$	error on $W_{\text{mx}}$ $\text{km s}^{-1}$	inclination degrees	$V_{\text{max}}$ $\text{km s}^{-1}$	$M_{\text{HI}}/M_{\odot}$ $10^{10}$ solar mass units	morph. type	$\log(d_{25})$ in log of 0.1 arcmin
17625	NGC1961	J054204.8+692243	3935	658	8	47.0	449.86	4.46	4.2	1.65
9560	NGC0958	J023042.8-025621	5739	570	10	78.1	291.26	3.77	4.9	1.40
14030	UGC02885	J035302.4+353522	5804	556	8	62.4	313.70	3.35	5.2	1.63
8066	NGC0812	J020651.6+443418	5161	435	16	71.9	228.82	3.24	5.9	1.44
64458	UGC11537	J201838.1-000902	5418	499	8	69.7	266.02	3.09	5.3	1.18
34836	NGC3646	J112143.1+201011	4246	508	16	63.9	282.84	2.96	4.6	1.49
52328	NGC5720	J143833.3+504855	7784	409	17	52.1	259.16	2.80	3.0	1.28
56891	ESO136-016	J160349.3-605840	5426	521	12	90.0	260.50	2.76	5.2	1.52
24830	UGC04625	J085017.8+032951	8476	422	18	90.0	211.00	2.74	6.1	1.23
62178	NGC6674	J183833.9+252230	3429	431	16	62.9	242.08	2.63	3.0	1.60
16537	UGC03218	J050043.7+621439	5228	495	15	56.4	297.15	2.62	3.1	1.24
59884	IC4633	J171346.9-773210	2945	318	13	62.4	179.42	2.57	6.0	1.43
61791	ESO395-002	J182226.4-354040	5607	538	13	90.0	269.00	2.56	3.4	1.32
19531	NGC2280	J064449.1-273819	1897	384	7	66.2	209.84	2.49	5.9	1.81
7387	NGC0753	J015742.2+355457	4902	314	8	52.5	197.89	2.41	4.9	1.14
52361	UGC09437	J143910.6+184247	14401	404	16	65.6	221.81	2.38	3.3	0.90
54250	NGC5833	J151153.6-725134	3031	407	14	76.7	209.11	2.36	4.2	1.49
9399	NGC0931	J022814.5+311840	4999	422	9	81.3	213.45	2.30	3.6	1.39
18089	UGC03375	J055525.3+515438	5791	490	11	64.2	272.13	2.29	5.2	1.18
28196	NGC2998	J094843.6+440453	4772	374	7	61.8	212.18	2.27	5.2	1.39

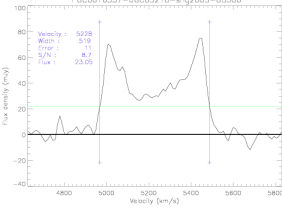
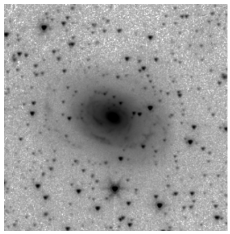
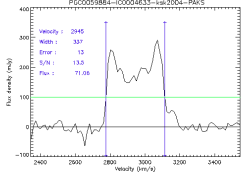
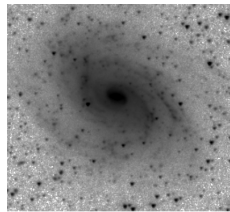
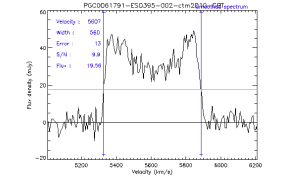
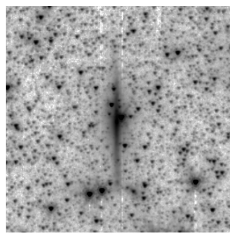
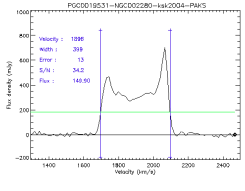
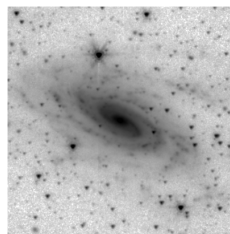
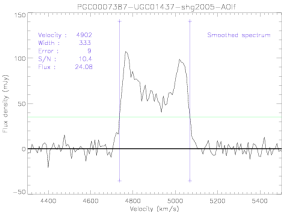
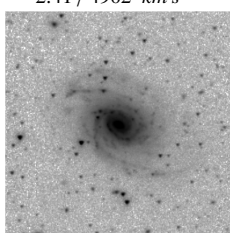
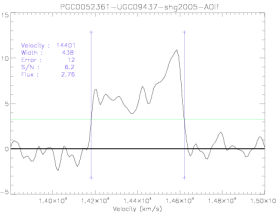
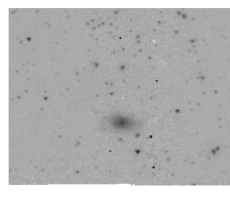
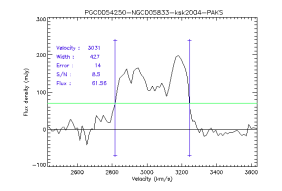
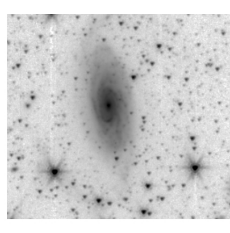
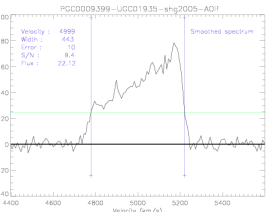
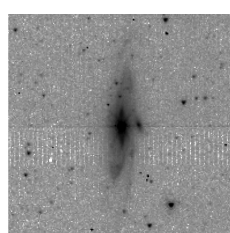
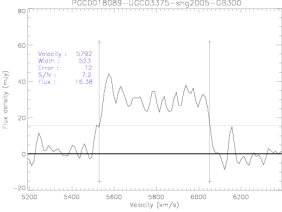
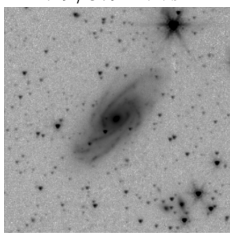
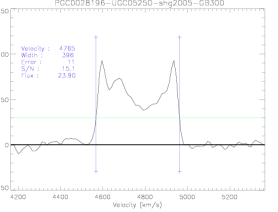
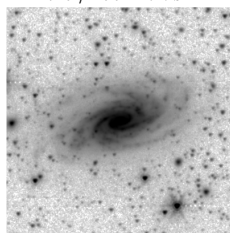
**Table 3.** The 20 fastest rotators

PGC	Name	J2000 coord.	$V_{hel}$ $km\ s^{-1}$	$W_{max}$ $km\ s^{-1}$	error on $W_{max}$ $km\ s^{-1}$	inclination degrees	$V_{max}$ $km\ s^{-1}$	$M_{HI}/M_{\odot}$ $10^{10}$ solar mass units	morph. type	$\log(d_{25})$ log of 0.1 arcmin
17625	NGC1961	J054204.8+692243	3935	658	8	47.0	449.86	4.46	4.2	1.65
42407	NGC4594	J123959.4-113723	1095	733	17	59.4	425.80	0.0430	1.1	1.93
63575	NGC6824	J194340.7+560634	3549	544	12	45.8	379.41	0.148	2.3	1.28
9359	NGC0936	J022737.4-010921	1436	545	11	50.5	353.15	0.0907	-1.2	1.65
165398	PGC165398	J043157.1+592547	4626	489	20	45.5	342.80	0.440	0.0	0.94
58596	NGC6195	J163632.6+390141	9021	517	18	50.2	336.47	0.221	3.1	1.16
65375	NGC6962	J204719.1+001915	4222	475	13	45.0	335.88	1.12	1.7	1.43
24685	ESO563-021	J084717.0-200208	4582	664	7	90.0	332.00	2.17	4.3	1.48
26512	NGC2841	J092202.5+505837	633	592	12	65.2	326.07	0.236	3.0	1.84
25161	NGC2713	J085720.5+025517	3916	629	18	77.7	321.89	0.503	2.5	1.53
36706	NGC3884	J114612.2+202330	6947	462	20	45.9	321.67	0.660	0.6	1.28
52665	NGC5746	J144456.0+015717	1723	634	11	90.0	317.00	0.456	3.0	1.86
57173	UGC10205	J160640.2+300556	6562	541	20	59.0	315.58	0.725	1.0	1.16
14030	UGC02885	J035302.4+353522	5804	556	8	62.4	313.70	3.35	5.2	1.63
37617	NGC3992	J115735.9+532228	1048	459	8	47.4	311.78	0.218	4.0	1.91
72233	UGC12755	J234349.7+282021	8794	503	19	54.7	308.16	0.648	3.1	1.07
67966	UGC11893	J220406.7+355618	5589	606	20	80.2	307.48	0.924	6.3	0.81
66880	UGC11758	J213057.6+135910	8635	612	19	90.0	306.00	0.942	4.2	1.12
45947	NGC5032	J131327.0+274808	6413	524	19	59.5	304.08	0.212	3.0	1.29
63286	UGC11455	J192956.3+720646	5392	608	15	90.0	304.00	1.29	5.8	1.39

**Table 4.** HI-21cm spectrum and Spitzer 3.6 $\mu$  images of the top 20 most heavy HI-mass galaxies, in decreasing mass order.

PGC - Name Telescope / HI profile	HI mass ( $\log(M_{HI})$ ) in solar units and $V_{hel}$ Spitzer 3.6 $\mu$ IRAC 400X400 pixels	PGC - Name Telescope / HI profile	HI mass ( $\log(M_{HI})$ ) in solar units and $V_{hel}$ Spitzer 3.6 $\mu$ IRAC 400X400 pixels
<p><b>PGC17625</b></p>  <p>GBT</p>	4.46 / 3935 $km s^{-1}$	<p><b>PGC9560</b></p>  <p>Parkes 64m</p>	3.77 / 5739 $km s^{-1}$
<p><b>PGC14030</b></p>  <p>GBT</p>	3.35 / 5804 $km s^{-1}$	<p><b>PGC8066</b></p>  <p>GB300</p>	3.24 / 5161 $km s^{-1}$
<p><b>PGC64458</b></p>  <p>GB300</p>	3.09 / 5418 $km s^{-1}$	<p><b>PGC34836</b></p>  <p>GB140</p>	2.96 / 4246 $km s^{-1}$
<p><b>PGC52328</b></p>  <p>GB300</p>	2.80 / 7784 $km s^{-1}$	<p><b>PGC56891</b></p>  <p>Parkes 64 m</p>	2.76 / 5426 $km s^{-1}$
<p><b>PGC24830</b></p>  <p>Arecibo</p>	2.74 / 8476 $km s^{-1}$	<p><b>PGC62178</b></p>  <p>GB140</p>	2.63 / 3429 $km s^{-1}$

**Table 5.** Table 4 .. continued ...HI-21cm spectrum and Spitzer 3.6 $\mu$  images of the top 20 most heavy HI-mass galaxies, in decreasing mass order.

PGC - Name Telescope / HI profile	HI mass ( $\log(M_{HI})$ ) in solar units and $V_{hel}$ - Spitzer 3.6 $\mu$ IRAC 400X400 pixels	PGC - Name Telescope / HI profile	HI mass ( $\log(M_{HI})$ ) in solar units and $V_{hel}$ - Spitzer 3.6 $\mu$ IRAC 400X400 pixels
PGC16537  GB300	2.62 / 5228 $km s^{-1}$ 	PGC59884  Parkes 64m	2.57 / 2945 $km s^{-1}$ 
PGC61791  GBT	2.56 / 5607 $km s^{-1}$ 	PGC19531  Parkes 64m	2.49 / 1897 $km s^{-1}$ 
PGC7387  Arecibo	2.41 / 4902 $km s^{-1}$ 	PGC52361  Arecibo	2.38 / 14401 $km s^{-1}$ 
PGC54250  Parkes 64m	2.36 / 3031 $km s^{-1}$ 	PGC9399  Arecibo	2.30 / 4999 $km s^{-1}$ 
PGC18089  GB300	2.29 / 5791 $km s^{-1}$ 	PGC28196  GB300	2.27 / 4772 $km s^{-1}$ 

## REFERENCES

- Aumer M., White S. D. M., 2013, *MNRAS*, 428, 1055
- Berlind A. A., Blanton M. R., Hogg D. W., Weinberg D. H., Davé R., Eisenstein D. J., Katz N., 2005, *ApJ*, 629, 625
- Berlind A. A., Weinberg D. H., 2002, *ApJ*, 575, 587
- Bernardi M., Roche N., Shankar F., Sheth R. K., 2011, *MNRAS*, 412, L6
- Blanton M. R. et al., 2003, *ApJ*, 594, 186
- Boselli A., Gavazzi G., 2006, *PASP*, 118, 517
- Bregman J. N., 2007, *ARA&A*, 45, 221
- Bullock J. S., Dekel A., Kolatt T. S., Kravtsov A. V., Klypin A. A., Porciani C., Primack J. R., 2001, *ApJ*, 555, 240
- Bundy K. et al., 2006, *ApJ*, 651, 120
- Burstein D., Bender R., Faber S., Nolthenius R., 1997, *AJ*, 114, 1365
- Cappellari M. et al., 2012, *Nature*, 484, 485
- Cattaneo A., Dekel A., Devriendt J., Guiderdoni B., Blaizot J., 2006, *MNRAS*, 370, 1651
- Conroy C., Wechsler R. H., 2009, *ApJ*, 696, 620
- Courtois H. M., Hoffman Y., Tully R. B., Gottlöber S., 2012, *ApJ*, 744, 43
- Courtois H. M., Pomarède D., Tully R. B., Hoffman Y., Courtois D., 2013, *AJ*, 146, 69
- Courtois H. M., Tully R. B., 2015, *MNRAS*, 447, 1531
- Courtois H. M., Tully R. B., Fisher J. R., Bonhomme N., Zavodny M., Barnes A., 2009, *AJ*, 138, 1938
- Courtois H. M., Tully R. B., Makarov D. I., Mitronova S., Koribalski B., Karachentsev I. D., Fisher J. R., 2011, *MNRAS*, 414, 2005
- Cybulski R., Yun M. S., Fazio G. G., Gutermuth R. A., 2014, *MNRAS*, 439, 3564
- Dale D. A. et al., 2009, *ApJ*, 703, 517
- De Lucia G., Weinmann S., Poggianti B. M., Aragón-Salamanca A., Zaritsky D., 2012, *MNRAS*, 423, 1277
- Dekel A., Birnboim Y., 2006, *MNRAS*, 368, 2
- Eggen O. J., Lynden-Bell D., Sandage A. R., 1962, *ApJ*, 136, 748
- Eskew M., Zaritsky D., Meidt S., 2012, *AJ*, 143, 139
- Fazio G. G. et al., 2004, *ApJS*, 154, 10
- Fischer P. et al., 2000, *AJ*, 120, 1198
- Freedman W. L., Madore B. F., 2010, *ARA&A*, 48, 673
- Freeman K. C., 1999, in *Astronomical Society of the Pacific Conference Series*, Vol. 170, *The Low Surface Brightness Universe*, Davies J. I., Impey C., Phillips S., eds., p. 3
- Gao L., Springel V., White S. D. M., 2005, *MNRAS*, 363, L66
- Geha M., Blanton M. R., Masjedi M., West A. A., 2006, *ApJ*, 653, 240
- Giovanelli R., Haynes M. P., Rubin V. C., Ford, Jr. W. K., 1986, *ApJ*, 301, L7
- Gómez P. L. et al., 2003, *ApJ*, 584, 210
- Governato F., Willman B., Mayer L., Brooks A., Stinson G., Valenzuela O., Wadsley J., Quinn T., 2007, *MNRAS*, 374, 1479
- Haynes M. P. et al., 2011, *AJ*, 142, 170
- Hoffman Y., Metuki O., Yepes G., Gottlöber S., Forero-Romero J. E., Libeskind N. I., Knebe A., 2012, *MNRAS*, 425, 2049
- Huchra J. P. et al., 2012, *ApJS*, 199, 26
- Kaiser N., 1987, *MNRAS*, 227, 1
- Kassin S. A. et al., 2007, *ApJ*, 660, L35
- Kauffmann G. et al., 2003, *MNRAS*, 341, 54
- Kennicutt R. C., Evans N. J., 2012, *ARA&A*, 50, 531
- Klypin A., Kravtsov A. V., Valenzuela O., Prada F., 1999, *ApJ*, 522, 82
- Knobel C. et al., 2013, *ApJ*, 769, 24
- McGaugh S. S., Schombert J. M., Bothun G. D., de Blok W. J. G., 2000, *ApJ*, 533, L99
- Meidt S. E. et al., 2014, *ApJ*, 788, 144
- Moore B., Ghigna S., Governato F., Lake G., Quinn T., Stadel J., Tozzi P., 1999, *ApJ*, 524, L19
- Muñoz-Mateos J., et al., 2015, *ApJS*
- Noordermeer E., Verheijen M. A. W., 2007, *MNRAS*, 381, 1463
- Obreschkow D., Ma X., Meyer M., Power C., Zwaan M., Staveley-Smith L., Drinkwater M. J., 2013, *ApJ*, 766, 137
- Peacock J. A., Smith R. E., 2000, *MNRAS*, 318, 1144
- Peebles P. J. E., 1976, *ApJ*, 205, L109
- Peng Y.-j., Lilly S. J., Renzini A., Carollo M., 2012, *ApJ*, 757, 4
- Querejeta M., et al., 2015, *ApJ* suppl. in press arXiv1410.0009
- Sales L. V., Navarro J. F., Theuns T., Schaye J., White S. D. M., Frenk C. S., Crain R. A., Dalla Vecchia C., 2012, *MNRAS*, 423, 1544
- Schombert J., 2007, ArXiv 0703646 and 2011ascl.soft07011S
- Sheth R. K. et al., 2010, *PASP*, 122, 1397
- Sheth R. K., Tormen G., 2004, *MNRAS*, 350, 1385
- Sorce J. G., Courtois H. M., Tully R. B., 2012, *AJ*, 144, 133
- Tinker J. L., George M. R., Leauthaud A., Bundy K., Finoguenov A., Massey R., Rhodes J., Wechsler R. H., 2012, *ApJ*, 755, L5
- Tully R. B., Courtois H., Hoffman Y., Pomarède D., 2014, *Nature*, 513, 71
- Tully R. B., Courtois H. M., 2012, *ApJ*, 749, 78
- Tully R. B. et al., 2013, *AJ*, 146, 86
- Tully R. B., Fisher J. R., 1977, *A&A*, 54, 661
- Tully R. B., Rizzi L., Shaya E. J., Courtois H. M., Makarov D. I., Jacobs B. A., 2009, *AJ*, 138, 323
- van Dokkum P. G., Conroy C., 2010, *Nature*, 468, 940
- Verheijen M. A. W., 2001, *ApJ*, 563, 694
- Walker M. A., 1999, *MNRAS*, 308, 551
- Wang J. et al., 2011, *MNRAS*, 413, 1373
- Wechsler R. H., Zentner A. R., Bullock J. S., Kravtsov A. V., Allgood B., 2006, *ApJ*, 652, 71
- Weiner B. J. et al., 2006, *ApJ*, 653, 1049
- Werner M. W. et al., 2004, *ApJS*, 154, 1
- Woo J. et al., 2013, *MNRAS*, 428, 3306
- Zaritsky D., 2012, *ISRN Astronomy and Astrophysics*, 2012, 12
- Zaritsky D., Colucci J. E., Pessev P. M., Bernstein R. A., Chandar R., 2012, *ApJ*, 761, 93
- Zaritsky D., Colucci J. E., Pessev P. M., Bernstein R. A., Chandar R., 2014a, *ApJ*, 796, 71
- Zaritsky D. et al., 2014b, *AJ*, 147, 134
- Zaritsky D., Gonzalez A. H., Zabludoff A. I., 2006, *ApJ*, 638, 725
- Zaritsky D., White S. D. M., 1994, *ApJ*, 435, 599
- Zaritsky D., Zabludoff A. I., Gonzalez A. H., 2008, *ApJ*, 682, 68
- Zwaan M. A., Meyer M. J., Staveley-Smith L., Webster R. L., 2005, *MNRAS*, 359, L30